

# Aptamer- and Fab'- Functionalized Microring Resonators for Aflatoxin M1 Detection

Tatevik Chalyan, Laura Pasquardini, Davide Gandolfi, Romain Guider, Alina Samusenko, Manuela Zanetti, Georg Pucker, Cecilia Pederzoli, and Lorenzo Pavesi, *Senior Member, IEEE*

**Abstract**—Silicon oxynitride (SiON) microring resonators are used to develop a biosensor device to detect Aflatoxin M1 (AFM1), a carcinogenic mycotoxin present in milk. Two different surface functionalization strategies are tested to realize an affinity biosensing device. Both strategies are based on the formation of a silane surface layer able to bind either specific DNA-aptamers or antigen binding fragments (Fab'). The sensing device consists of an array of four SiON microring resonators, fiber-coupled to a vertical cavity surface emitting laser operating at 850 nm. Detection is realized with off-chip silicon photodetectors. With both functionalizations, we demonstrate a specific detection of AFM1 in buffer, while the nonspecific detection of Ochratoxin is not occurring. Repeatability and reproducibility of both functionalization strategies are discussed.

**Index Terms**—Aflatoxin M1, antibodies, aptamers, microring resonators.

## I. INTRODUCTION

**A**FLATOXINS (AFs) are known as poisonous and carcinogenic mycotoxins present in a variety of crops, which can be infected pre-, during and post-harvest [1]. They were discovered for the first time in 1960 in England. AFs are found in many human or animal foods. Since they are very resistant toxins and resist to chemical or thermal treatments, they do represent a particular hurdle for human alimentation. In particular, when ingested by animals, AFs can maintain their toxicity and find themselves in the animal metabolism products. For example, Aflatoxin B1 (AFB1), when ingested by cows, is converted in a hydroxylated metabolite and secreted into the milk. In this case, AFs is named Aflatoxin M1 (AFM1). AFM1 is also observed in dairy products. The International Agency for Research on Cancer (IARC) has included AFM1 in the group I human carcinogens [2]. Acceptable maximum level of

Manuscript received June 1, 2016; revised September 7, 2016; accepted September 7, 2016. This work was supported by the FP7 EU project "SYMPHONY" (Grant agreement no: 610580).

T. Chalyan, D. Gandolfi, R. Guider, and L. Pavesi are with the Nanoscience Laboratory, Department of Physics, University of Trento, Povo 38123, Italy (e-mail: tatevik.chalyan@unitn.it; davide.gandolfi@unitn.it; rom.guider@gmail.com; lorenzo.pavesi@unitn.it).

L. Pasquardini was with LaBSSAH, Fondazione Bruno Kessler, Povo 38123, Italy. She is now with the Department of Engineering, University of Trento, Povo 38123, Italy (e-mail: l.pasquardini@gmail.com).

A. Samusenko and G. Pucker are with the Center for Material and Microsystems, Bruno Kessler Foundation, Trento 38123, Italy (e-mail: samusenko@fbk.eu; pucker@fbk.eu).

M. Zanetti and C. Pederzoli are with the LaBSSAH, Fondazione Bruno Kessler, Povo 38123, Italy (e-mail: mzanetti@fbk.eu; pederzo@fbk.eu).

Color versions of one or more of the figures in this paper are available online at <http://ieeexplore.ieee.org>.

Digital Object Identifier 10.1109/JSTQE.2016.2609100

TABLE I  
BIOSENSORS FOR AFM1 DETECTION

Name	LOD of AFM1 (nM)	Cons and Pros	Ref.
ELISA	$1.31 \times 10^{-2}$	High selectivity, portable, expensive, time consuming	[6], [8]
HPLC	$1.37 \times 10^{-2}$	High selectivity, expensive, time consuming, non-portable, needs sample pre-treatment	[7], [9]
Electrochemical Biosensor	$3.04 \times 10^{-2}$	High selectivity, expensive, fast, needs sample pre-treatment and pre-concentration	[10]
Field immunoassay	$1.52 \times 10^{-1}$	High selectivity, low-cost, fast, easy to use, non-portable	[11]
Microelectrode immunosensors	$2.43 \times 10^{-2}$	High selectivity, low-cost, time consuming, non-portable	[12]
SPR	$1.82 \times 10^{-3}$	High selectivity, expensive, fast, non-portable	[13]
Bilayer lipid membranes (BLM)	$4.9 \times 10^{-2}$	High selectivity, low-cost, fast, small, portable	[14]
MRR based biosensors	5	High selectivity, low-cost, fast, small, portable, multianalyte, needs sample pre-concentration	This work

AFM1 in milk according to EU regulation is 50 ppt equivalent to  $15.2 \times 10^{-2}$  nM (the molecular weight of AFM1 is 328.27 g/mol) [3].

Methods for AFM1 determination in milk are mostly based on high-performance liquid chromatography associated to fluorescence or mass spectrometric detection [4]–[5]. Milk samples are analyzed in biochemistry laboratories with screening tests, such as Enzyme-Linked Immunosorbent Assay (ELISA) [6]. Samples with suspect presence of aflatoxins are then sent to certificate laboratory for High-Performance Liquid Chromatography (HPLC) tests [7]. This analysis is time-consuming and cost intensive.

Numerous strategies, alternative to both ELISA and HPLC, have been proposed for the rapid, qualitative, semi-quantitative or quantitative detection of AFs (see Table I).

Looking for a simple and effective method to screen the presence of AFM1 in milk, we have started a project to develop an integrated silicon-photonics biosensor [15]–[16]. Integrated optical biosensors are suitable for real time detection of molecular interactions [17] owing to their possibility of miniaturization, extreme sensitivity (molecular interactions), robustness, reliability, and their potential for multiplexing and mass production at low cost. In particular, label-free optical biosensors are based on the selective capture of the target molecule (analyte) by a bio-recognition agent, immobilized on the surface of the sensor. The trapped molecules form a layer whose presence on the

sensor surface can be directly measured by quantifying the changes in a property of the transmission spectrum of the optical sensor [18]. By miniaturizing the sensing sites, it is possible to limit the volumes of the samples and of the chemicals involved in the functionalization protocol, thus reducing the costs and the time of every assay. The device itself can be cheap because a high number of multiplexed sensors can be fitted and run in parallel in a small area, as small as a few square millimeters [19].

In this work, we demonstrate an optical biosensor based on optical microring resonators (MRR) [20], [22]. Here, the sensing is performed by measuring the resonance shift in the MRR transmission caused by the binding of the analyte on the functionalized microring surface. In fact, the binding causes a change of the effective refractive index,  $n_{\text{eff}}$ , of the optical mode confined in the MRR, which, in turn, is observed as a resonance shift in the MRR transmission [23]. MRR based optical sensors have already been demonstrated for a variety of applications, and, specifically in food safety applications [24]–[25].

Selectivity in the sensor response is achieved by using a surface functionalization with a suitable biorecognition agent. To this aim, antibodies have been widely used due to their Y-shaped structure that ends with two particular antigen-binding sites [26]. These sites can bind to their specific antigen through a key-lock mechanism. On the other end, aptamers are emerging as alternatives to antibodies [27]. Aptamers are short single-stranded DNA or RNA molecules, or even peptides, having high selectivity and affinity toward their targets. Aptamers are chemically synthesized and, therefore, are stable and easily modified. Their denaturation is reversible, allowing for regeneration of the active sensing site. Moreover, their small dimensions allow a high-density coverage of the sensor surface [28].

This paper aims to experiment silicon based MRR as biosensor to selectively detect AFM1 in a buffer solution. We compare two functionalization strategies, Fab'-based antibodies and DNA-aptamers. First, the two strategies are set up on flat silicon oxynitride surface and are compared in terms of AFM1 recognition using an HRP-conjugated Aflatoxin M1. Then, label-free measurements on functionalized microring resonators are performed.

## II. MATERIALS AND METHODS

### A. Materials

3-mercaptopropyltrimethoxysilane (MPTMS, 99%) purchased from Gelest Ltd. (Maidstone, Kent, United Kingdom), is used without any further purification. 3-glycidioxypropyltrimethoxysilane (GPTMS), anhydrous toluene (99.8%), toluene and all powders for buffered solutions are purchased from Sigma-Aldrich s.r.l. (Milan, Italy). Methoxypolyethyleneglycolthiol (mPEG-SH) with 2000 and 5000 molecular weight are purchased from Nektar Therapeutics AL (Huntsville, AL). The amino-modified DNA-aptamer sequence (5'-NH<sub>2</sub>-(CH<sub>2</sub>)<sub>6</sub>-GT TGG GCA CGT GTT GTC TCT CTG TGT CTC GTG CCC TTC GCT AGG CCC ACA-3') with a fluorescein dye at 3' end or not, is HPLC purified and is purchased from IDT Integrated DNA Technologies (Leuven, Belgium). The aptameric sequence, which has a dissociation constant  $K_D$  of 10 nM, is

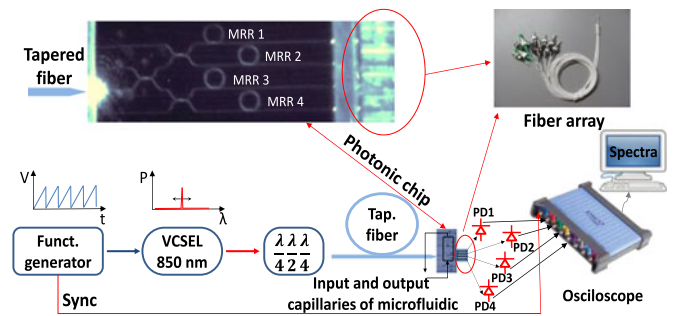


Fig. 1. (Top left) image of the chip during operation. On the left, the bright spot is the laser scattering at the input waveguide. On the right, the fiber array is visible. On the chip, the location of the four microring resonator is indicated. (Bottom) Schematic of the experimental setup.

identified by NeoVentures Biotechnology Inc [28]. A rabbit polyclonal anti-AFM1 antibody and an HRP-conjugated aflatoxin M1 (AFM1-HRP) contained in the I'screen Afla M1 milk Elisa kit are purchased from Tecna s.r.l. (Padua, Italy), while Aflatoxin M1 and Ochratoxin were purchased from Sigma-Aldrich s.r.l. (Milan, Italy). SuperSignal West Femto Chemiluminescent Substrate is purchased from Thermo Scientific (Rockford, IL USA).

### B. Fabrication Process

For the fabrication of the microring resonators, SiON films are deposited by plasma-enhanced chemical vapor deposition (PECVD) on 6-inch 625  $\mu\text{m}$  thick c-Si wafers with a 4  $\mu\text{m}$  thick buffer oxide layer. The SiON film thickness is 350 nm, its refractive index is 1.66. Both values are measured after a thermal treatment at 1050  $^{\circ}\text{C}$ . The SiON waveguide circuit, consisting of waveguides, splitters and microring resonators (Fig. 1 top left), is realized with UV-photolithography and reactive ion etching. Then, the SiON is covered by a 1  $\mu\text{m}$  thick cladding layer in silicon dioxide (SiO<sub>2</sub>). The sensor sites are defined by opening a 20  $\mu\text{m}$ -wide window on top of the ring resonators using a combination of reactive ion etching and chemical etching. More details on the fabrication process of the waveguides, resonators and directional couplers are reported in [29]–[30].

### C. Experimental Setup and Sensor Design

To measure the resonance shift induced by the presence of the toxin, a waveguide-probing setup is used. A single mode tapered fiber is coupled to input of the chip while a fiber array is coupled to the chip outputs. The fiber array allows measuring simultaneously the transmission of four different microrings (see Fig. 1). As a light source we use a current controlled VCSEL pigtailed to the single mode fiber and operating at 850 nm. This wavelength is particularly interesting for biosensing application since the absorption of water is three orders of magnitude lower in the visible/near-infrared range than in the infrared range. This wavelength allows also using cheap transimpedance amplified Si photodiodes. The signal polarization is controlled by using a 2-paddles polarization controller. For sensitivity and sensing measurements, a homemade PDMS microfluidic flow cell is used, with capillaries having a diameter of 150  $\mu\text{m}$ . PDMS

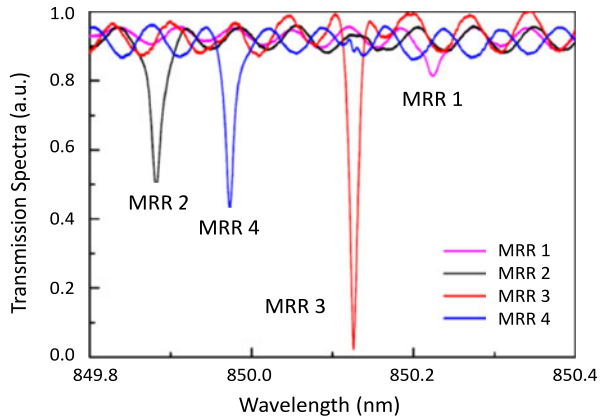


Fig. 2. Transmission spectra of four microring resonators. MRR1 is covered by the cladding, while the other three are exposed to water.

is chosen to satisfy several requirements. The cell has to be transparent, in order to be easily aligned to the sensing structures and it should seal with the chip to avoid a leakages. Finally, data are acquired with an eight-channel oscilloscope from Pico Technology interfaced with a computer. Spectral measurements are acquired by driving the VCSEL with a periodic saw tooth current waveforms (frequency 20 Hz). A software allows to deduce in real time the resonance spectral position from the measured transmission spectra, and, therefore, to plot the time evolution of the resonance spectral shift.

On the chip, the signal from the input waveguide is coupled to four microring resonators (MRR) by directional couplers (see the top left image in Fig. 1). A racetrack resonator geometry is used for the MRR with a coupling length of 35  $\mu\text{m}$ , a radius of 100  $\mu\text{m}$  and a resonator waveguide width of 1000 nm. The width of the bus waveguide is fixed to 900 nm. Details of the optimization of the geometry and of the actual design are reported in [22], [29].

The  $\text{SiO}_2$  cladding is removed from three of the four MRR to open a sensing window. The first MRR (labelled MRR 1) is left covered by the cladding in order to isolate it from the microfluidic chamber and, therefore, to be used as the reference sensor (baseline sensor) for the input signal intensity and to measure temperature fluctuations. Suitable spacing between the sensors is left so that it is possible to use a spotter to functionalize each individual sensor with a different chemistry allowing internal consistency tests or multianalyte detection.

Fig. 2 shows the transmission spectra of the four nominally identical MRR under a continuous water flow. Clear sharp resonances are observed. The different resonance wavelengths are caused by small fabrication uncertainties. Since the sensor works on the resonance shift caused by the binding of the toxins, this does not affect the sensing properties. The oscillations are due to the Fabry-Perot interference fringes caused by the chip facets.

### III. FUNCTIONALIZATION PROTOCOL

#### A. DNA-Aptamers Immobilization

The first functionalization protocol has been already described with details in [21]. Briefly, after an argon plasma

treatment (6.8 W, one minute), the samples are immersed in 0.1% v/v of GPTMS in anhydrous toluene at 60  $^\circ\text{C}$  for 10 minutes. Then, an amino-terminated DNA-aptamer at 100  $\mu\text{M}$  in phosphate buffer (50 mM, ionic strength 300 mM, pH 8) is incubated on silanized surfaces for two hours. Finally, an ethanolamine passivation at 1 mM for 30 minutes is applied.

#### B. Antigen-Binding Fragments (Fab') Functionalization

The second protocol is based on a silanization and antigen-binding fragments (Fab') immobilization on the chip.  $\text{F(ab')}_2$  fragments are generated by protease digestion (Immobilized Papain Thermo Scientific) of 20  $\mu\text{L}$  of 1 mg/mL anti-AFM1 polyclonal rabbit IgG according to manufacturer's instructions. Then, a 13.3  $\mu\text{M}$   $\text{F(ab')}_2$  solution is mixed with 10 mM DTT to reduce the disulfide bond in the hinge region, and the mixture is incubated for two hours at room temperature. The mixture is poured into a centrifugal filter unit (Microcon YM-10, MWCO 10000, Millipore Corp., Billerica, MA) to remove the excess of DTT.

Fab' are immobilized on the surface adapting the protocol described in [31]. In order to introduce thiol groups able to react with the cysteine groups on Fab' fragments, the silicon oxynitride surface is functionalized in wet conditions with mercaptosilane (MPTMS) [32]. The surfaces (both chip and flat samples) are cleaned with an argon plasma (6.8 W, one minute) to remove organic contaminants and to hydroxylate the surface and are, then, immersed in a 1% v/v solution of MPTMS in toluene anhydrous at 60  $^\circ\text{C}$  for 10 min. Silane-coated substrates are rinsed several times with toluene and then dried in a stream of nitrogen. The immobilization of Fab' fragments onto the bare surface is carried out by deposition of 80  $\mu\text{L}$  of a 0.33  $\mu\text{M}$  Fab' in 10 mM phosphate buffer with 10 mM EDTA. After 2 min, the surface is PEGylated by addition, first, of 200  $\mu\text{M}$  final concentration of mPEG-SH 5000 (for 30 min on orbital shaker at 80 rpm) and, then, of 200  $\mu\text{M}$  of mPEG-SH 2000 (for 60 min on shaker at 80 rpm). The surface is finally cleaned using PBS-EDTA buffer. The same protocol is applied on standard flat gold surface. The concentration of Fab' is determined by measuring their absorbance with a Nanodrop instrument, (extinction coefficient (0.1%) = 1.35 at 280 nm).

## IV. RESULTS AND DISCUSSIONS

#### A. Comparison of the Two Strategies on Flat Surfaces

The Fab' density on silanized SiON is optimized incubating different concentration. After immobilization, the surfaces are incubated with an HRP-conjugated Aflatoxin M1 (AFM1-HRP) stock solution diluted 80 times in 50 mM MES buffer pH 6.6 for one hour, washed twice in buffer and transferred to a black microplate, where the developer solution is added. HRP in presence of a suitable substrate develops a chemiluminescence signal that can be easily detected. After five min incubation, the signal is recorded with a ChemiDoc MP system (Biorad). Respect to a gold surface (a standard surface for thiol chemistry), a saturation of the surface is obtained at low Fab' concentration, as reported in Fig. 3(a). Fitting the data with a Langmuir equation, it is possible to determine the surface saturation. For

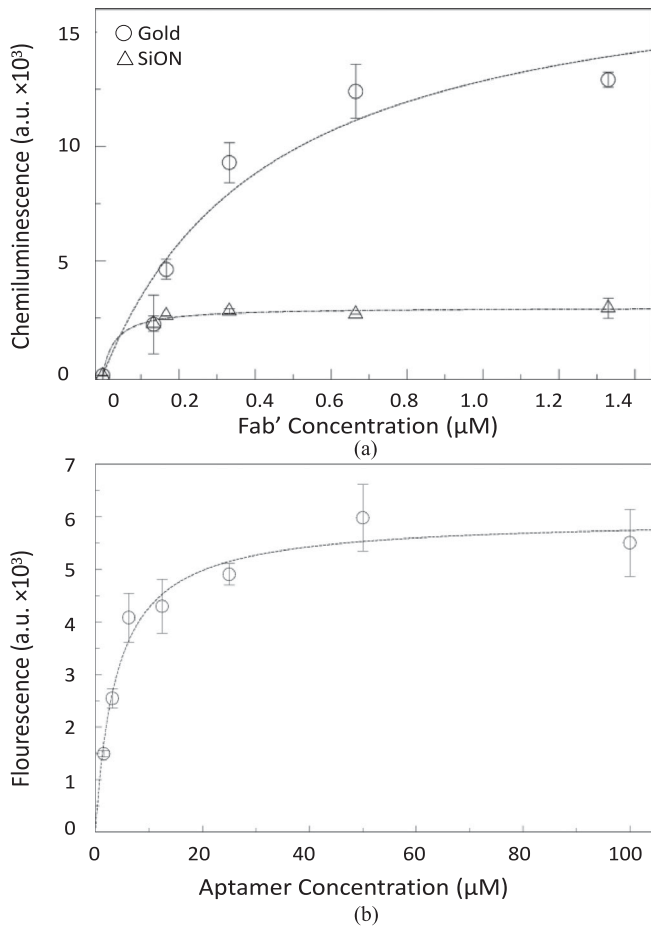


Fig. 3. (a) Chemiluminescence detection of AFM1-HRP on SiON substrates after immobilization of different amount of Fab'. A gold substrate is used as reference. The values are reported as mean value on at least two different experimental sessions and the error bars represent the standard deviation. (b) Fluorescence signal on SiON surface functionalized with different amount of fluorescent aptameric sequences. The values are reported as mean value on three different samples and the error bars represent the standard deviation.

SiON surface the value saturates at 2957 a.u. (correlation coefficient = 0.99), while for gold surface a 18588 a.u. value was estimated (correlation coefficient = 0.97). The signal recorded on silanized SiON surface is about 6 times lower than that recorded on gold, suggesting that the surface binding sites on mercaptosilanized SiON are fewer than those on gold surface, as expected. A 0.33  $\mu\text{M}$  Fab' concentration is selected for the following experiments.

The aptamer density is instead optimized using a fluorescein-labelled DNA aptameric sequence. The fluorescence signal is recorded after two hours of incubation and washing. Fig. 3(b) shows the fluorescence signal as a function of the aptamer concentration. Also in this case the Langmuir equation describes the aptamer immobilization. The saturation level resulted at 5970 a.u. (correlation coefficient = 0.98), suggesting that a concentration above 50  $\mu\text{M}$  is enough to reach the surface saturation. Then, the two functionalization procedures are compared with respect to their ability to recognize AFM1 by using AFM1-HRP. SiON flat substrates are functionalized with DNA-aptamers or Fab' and the surfaces are incubated with AFM1-HRP in the

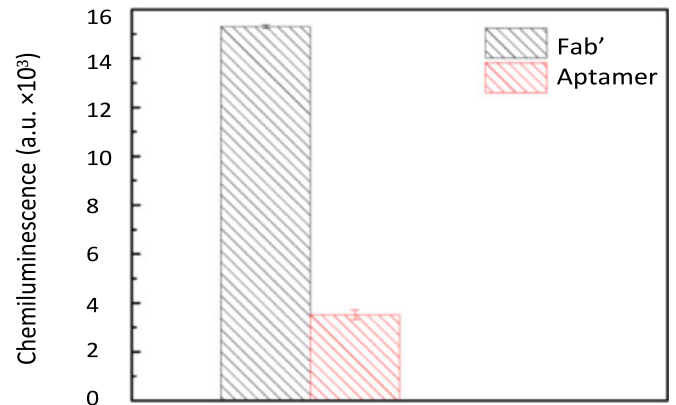


Fig. 4. Chemiluminescence detection of AFM1-HRP on silicon oxynitride flat surfaces functionalized with Fab' or aptamer strategy. The data are represented as mean value on three samples and error bars are reported as standard deviation.

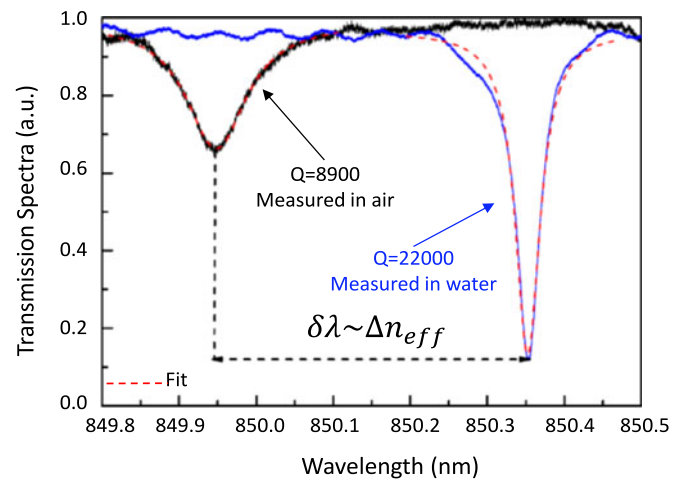


Fig. 5. Transmission spectra of microring resonator measured in the air (black curve) and water (blue curve). Q is the quality factor of the resonance. The dashed (red) line is the Lorentzian fit.

same conditions reported above. The signals recorded on the Fab'- or aptamer- functionalized surfaces are reported in Fig. 4. A higher signal is observed for the Fab'-functionalized surface. The AFM1 detection is about 4 times more efficient on the immune surface respect to the aptamer-functionalized surface.

### B. Optical Characterization of Microring Resonators

The design of the resonators was optimized for the biosensing experiments. Indeed, in Fig. 5 we show a transmission spectrum of one of the resonator when the chip is flown with air or with deionized water. A different transmission and Quality factor (Q-factor) are measured. For in air measurements, the decrease of the Q-factor for three neighboring resonances at longer wavelengths allows concluding that we are in the under-coupling regime. For in water measurements, a near critical coupling regime settles in with high Q-factors. The switch from under-coupling to critical coupling is a consequence of the change in the refractive index contrast from air to water. Fitting the transmission spectra with a Lorentzian lineshape, Q-factors of 8,900

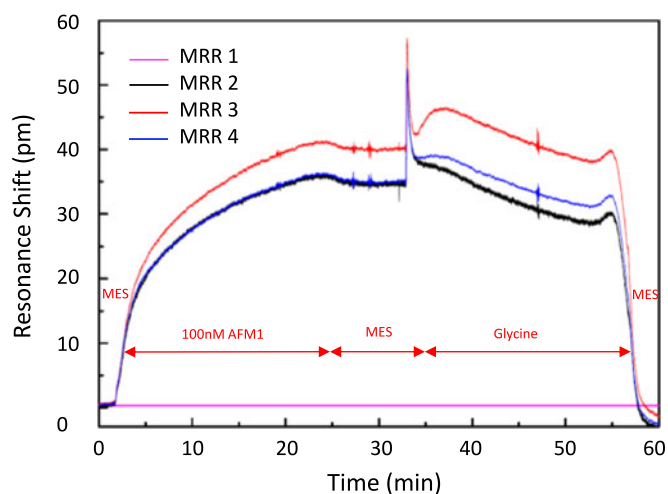


Fig. 6. Sensorgram of a complete measurement cycle for a chip sensor functionalized with Fab' and for a 100 nM AFM1 solution. At  $t = 0$ , MES buffer is flowing through the sensors. The toxin is injected at  $t = 2$  min and at  $t = 25$  min the toxin flow is stopped and the MES buffer is injected again. After 30 minutes a glycine solution is injected. At  $t = 55$  min MES buffer was injected again.

in air and of 22,000 in water are obtained. Therefore, a ratio of 2.5 between the two values is obtained. This ratio matches numerical simulations [23], [33].

Volumetric sensing measurements yield a sensitivity of  $S = 80 \pm 5$  nm/RIU and a LOD =  $3 \times 10^{-6}$  RIU [21], [22]. Note, that these values are in good agreement with sensitivity and LOD reported in other works [34].

### C. Aflatoxin M1 Sensing Measurements

For AFM1 sensing measurements, we initially filled the microfluidic chamber with a 50 mM MES buffer with pH 6.6. We then injected 75  $\mu$ L of a solution containing the targeted mycotoxin (AFM1 or OTA) at a known concentration in order to measure the evolution of the resonance wavelength of the resonators due to the capture of the toxins from the functionalized MRR. The solution is inserted into the microfluidic chamber using an injection loop, which avoids the formation of air bubbles in the microfluidic chamber during the buffer exchange and allows having a known fixed injected volume. All measurements are done with a flow rate of 3  $\mu$ L/min.

Fig. 6 shows an example of a sensorgram measured with a solution of 100 nM AFM1 when the surface of the MRR in the chip has been functionalized with Fab'.

The measurement starts with flowing the MES buffer. The resonance wavelengths of the three exposed sensors MRR2-MRR4 as well as that of the reference sensor MRR1 stay constant while flowing the buffer. We consider these values as the baseline. Then, we inject the 100 nM AFM1 solution. The solution reaches the sensor after 2 min when we observe a large resonance shift for MRR2-MRR4 while no shift is measured for the reference MRR1. This shows that no temperature fluctuations are caused by the change in the flown solution. The MRR2-MRR4 resonances roughly follow an exponential law, due to the specific binding of AFM1 to the functionalized surfaces of the three MRR. The binding of the toxins occur from

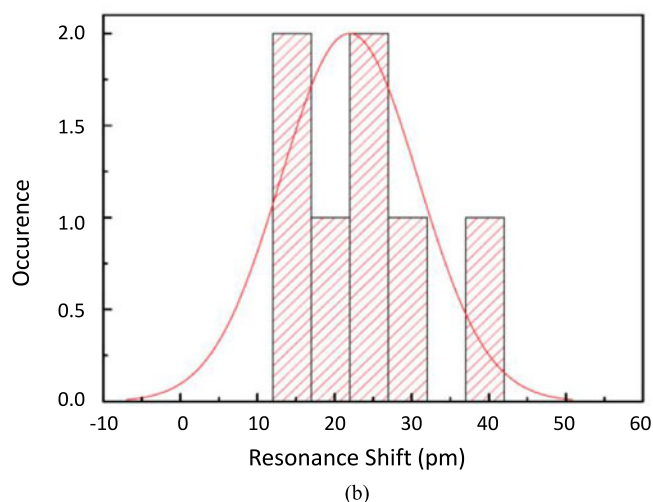
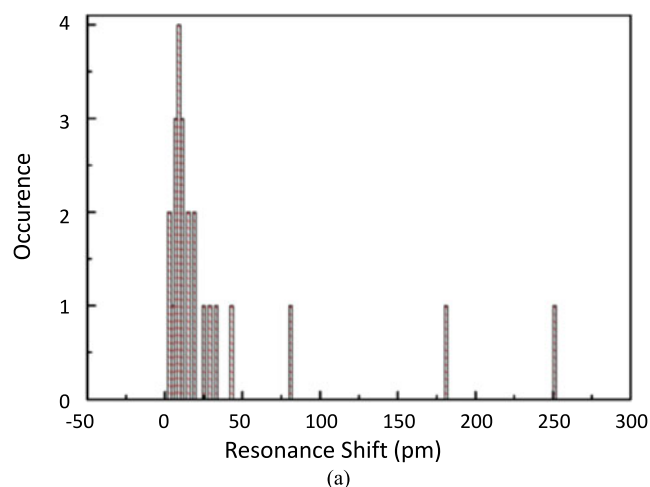


Fig. 7. (a) The histogram of the resonance shift of the microring resonator for aptamer based functionalization. The average resonance shift is 30 pm with an error of 59 pm. The solution used is 100 nM of AFM1. (b) The histogram of the resonance shift of the microring resonator for Fab' based functionalization. The average resonance shift is 25 nm with an error of 8.5 pm. The solution used is 100 nM of AFM1.

the 2.5 min and 25 min. At this time, we stop the toxins flow and we switch to a MES buffer flow. This causes a decrease in the resonance shift due to the rinsing of the physically absorbed AFM1 from the surface. Therefore, we consider indicative of the sensor response the value of the resonance shift after 22.5 minutes that is varying between  $33 \div 38$  pm for MRR2-MRR4. Finally, we inject a 100 mM glycine-HCl pH 2.3 solution at  $t = 30$  min, in order to break the AFM1-antibody bonds and to remove all the linked toxins from the sensor surface while keeping the antibodies in place. This regeneration solution is commonly used in surface binding experiments. It perturbs the aptamers or Fab' tridimensional conformation, which leads to a release of the captured toxins. After glycine solution, at  $t = 55$  min we inject again MES and the signals reach close to the baseline indicating that the sensors are again clean. Note that the MRR1 resonance does not shift during the whole cycle.

Fig. 7 shows the histograms of repeated measurements on different chips for the same functionalization protocols and the same AFM1 solution to test the reproducibility of the

sensor response from chip-to-chip. Fig. 7(a) shows the results for aptamer-functionalized MRRs when the concentration of injected AFM1 is 100 nM. As we can clearly observe, the resonance shift changes between 10 pm to 220 pm. The average value with standard deviation is  $\approx 33 \pm 59$  pm showing that the reproducibility of the measurements is poor. The source of this can be looked for in the wafer processing, in the functionalization procedure or in the toxin binding dynamics. Since wafer processing reproducibility is very high [22] and the surface functionalization gives reproducible results (see, e.g., Fig. 4), we conclude that the low reproducibility is related to the microfluidic and binding steps. Fig. 7(b) reports the same experiment for sensors functionalized with Fab'. The distribution of the resonance shifts on different chips is much narrower than with aptamer functionalization (between 15 pm and 42 pm) yielding an average value and a standard deviation of  $\approx 25 \pm 8.5$  pm. It is therefore concluded that the Fab' functionalization is more reproducible than the aptamer one.

In addition, we note that the average shifts are equal within the error bars for the two functionalizations. This differs from what observed with the surface experiments. There are several possible explanation for this. For the flat surface experiments, an enzyme-conjugated aflatoxin is used, while, for sensing measurements, a pure AFM1 is used. AFM1-HRP and the antibody used for Fab' production are part of the same Elisa assay. It could be that a higher affinity of Fab' for AFM1-HRP occurred with respect to aptamers. Another consideration relates to the sensor surfaces. Chemiluminescence detection of AFM1-HRP on SiON substrates gives direct information about bound molecules, while the detected signal of the microring sensors depends also on the thickness of the bound layer on the surface [23]. In fact, the volume of interaction between the analyte and the evanescent field of the MRR optical mode is constrained by the thickness of the layer of the captured analyte. In the case of nanometric-sized molecules, this means that most of the evanescent tail is unperturbed and not used to produce a signal. The molecular weight of Fab' is around 50 kg/mol, more than three times larger than the aptamers, while the molecular weight of AFM1 is 328.27 g/mol. The resulting bound layer is therefore far apart for the Fab'-based functionalization than for the aptamer-based functionalization which decreases the interaction between the evanescent tail and the small AFM1 molecules.

Fig. 8(a) shows the measured resonance shifts for various AFM1 concentrations. In order to obtain the minimum concentration of AFM1 that can be reliably detected, i.e. the limit of detection  $\text{LOD}_{\text{AFM1}}$  of the sensor to AFM1, we use a linear regression to the data (line in Fig. 8(a)) [35]. The slope of the linear regression yields the sensitivity of the sensor to AFM1, which is  $S_{\text{AFM1}} = 0.335 \pm 0.02$  pm/nM. From resonance measurements [34] we have a standard deviation of  $\sigma_{\lambda} = 0.08 \pm 0.005$  pm on the measured wavelength. This corresponds to a theoretical  $\text{LOD}_{\text{AFM1}} = 3\sigma_{\lambda}/S_{\text{AFM1}} = 0.7$  nM. Actually, if we consider the intercept of the linear regression as a best estimate of the error  $\sigma_{\text{AFM1}}$  in the concentration measurements, we obtain the experimental  $\text{LOD}_{\text{AFM1}} = 3\sigma_{\text{AFM1}}/S_{\text{AFM1}} \cong 5$  nM.

Fig. 8(b) shows various sensorgrams for different composition of the tested samples. Functionalization is specific to AFM1.

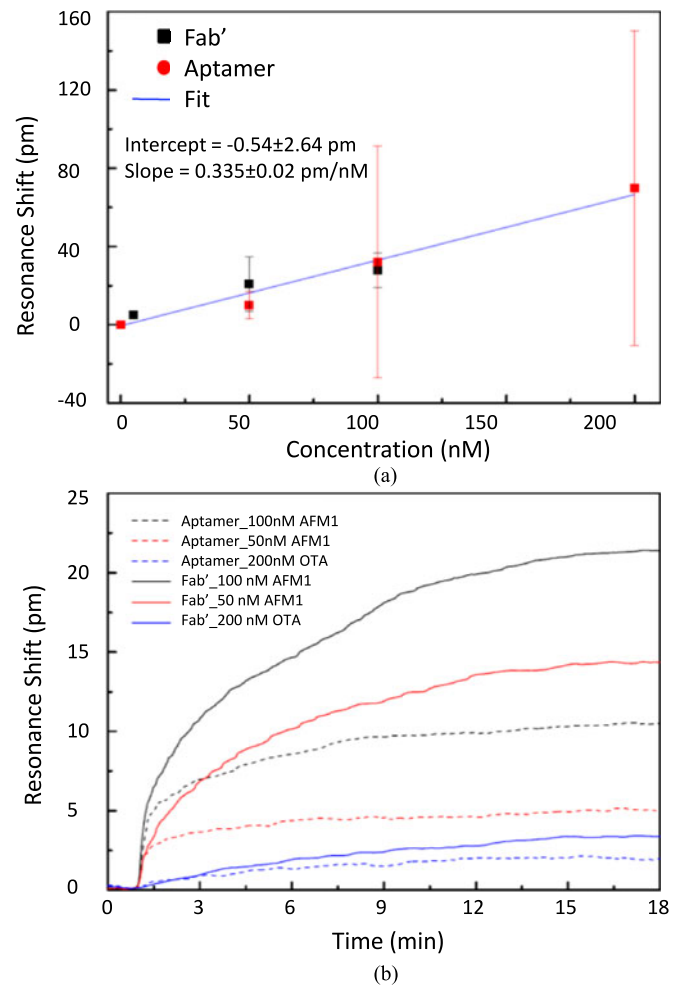


Fig. 8. (a) The resonance shift for different concentrations of AFM1 detected with Fab' (black squares) and aptamers (red circles) based functionalization. The line is a linear regression of the data. (b) Sensing measurements of 50 nM and 100 nM pure AFM1 and 200 nM OTA diluted in MES performed on sensors functionalized with both aptamer (dash lines) and Fab' (straight lines) based strategies. The flowing buffer is MES.

In order to test the specificity of the functionalization we tried the sensor with a solution containing OTA. We performed sensing measurements with AFM1 at 50 nM, 100 nM and OTA at 200 nM concentrations. Both mycotoxins are diluted in MES buffer. The protocol of the measurements is the same. For both functionalization strategies, the specificity is observed. However it is already showed above (see Fig. 7(a)) that a poor reproducibility has been observed using the aptamer-functionalized sensors and this is highlighted by the large error bars mainly at high AFM1 concentrations.

Indeed the resonance shift is small for OTA while it is larger for AFM1. Note again, that a higher reproducibility of Fab'-functionalized sensors was observed.

## V. CONCLUSION

In this work we demonstrate that Fab' based functionalization of SiON microring resonator based biosensors allows to specifically detect, down to 5 nM, Aflatoxin M1 in a MES buffer. The

Fab' functionalization yields more reproducible results with respect to the DNA aptamer functionalization. The specificity of the sensor functionalization to detect Aflatoxin M1 molecules is demonstrated with respect to non-specific Ochratoxin molecules at high concentrations. The limit of detection for the label-free biosensors is mostly limited by the reproducibility of the measurement from functionalized chip to functionalized chip. We believe that this is not related to the photonic circuit fabrication or to the functionalization but it is instead due to the interaction of the liquid sample with the biosensor.

The potential use of the proposed biosensor for cheap, fast and portable instrument to screen the presence of Aflatoxin M1 in milk requires the integration in the system of a preconcentration module since the high LOD demonstrated.

#### REFERENCES

- [1] L. Anfossi, C. Baggiani, C. Giovannoli, and G. Giraudi, "Lateral flow immunoassays for Aflatoxins B and G and for Aflatoxin M1," in *Aflatoxins - Recent Advances and Future Prospects*, M. Razzaghi-Abyaneh, Ed. Turin, Italy: InTech, 2013, ch. 15.
- [2] International Agency for Research on Cancer (IARC), "Evaluation of carcinogenic risks in humans," IARC, Lyon, France, 2002, pp. 171–274.
- [3] European Commission, "Commission Regulation (EC) No 1881/2006 of 19 December 2006 setting maximum levels for certain contaminants in foodstuffs," *Official J. Eur. Community*, L364, pp. 5–24, 2006.
- [4] M. Muscarella, M. S. Lo, C. Palermo, and D. Centonze, "Validation according to European Commission Decision 2002/657/EC of a confirmatory method for aflatoxin M1 in milk based on immunoaffinity columns and high performance liquid chromatography with fluorescence detection," *Analitica Chimica Acta*, vol. 594, no. 2, pp. 257–264, 2007.
- [5] W. L. Chen, T. F. Hsu, and C. Y. Chen, "Measurement of aflatoxin M1 in milk by ultra-high-performance liquid chromatography/tandem mass spectrometry," *J. AOAC Int.*, vol. 94, no. 3, pp. 872–877, 2011.
- [6] A. Biancardi, "Determination of aflatoxin M1 residues in milk. A comparative assessment of ELISA and IAC-HPLC methods," *XXXV Industrie Alimentari*, pp. 870–876, 1997.
- [7] P. Markaki and E. Melissari, "Occurrence of Aflatoxin M1 in commercial pasteurised milk determined with ELISA and HPLC," *Food Addit. Contam.*, vol. 14, no. 5, pp. 451–456, 1997.
- [8] M. Abouzied, P. Bentley, F. Klein, and J. Rice, "A sensitive ELISA for the detection and quantitation of Aflatoxin M1 (AFM1) in milk and dairy products," *Neogen Corp.*, Lansing, MI, USA.
- [9] A. Behfar *et al.*, "Determination of Aflatoxin M1 levels in produced pasteurized milk in Ahvaz City by using HPLC," *Jundishapur J. Nat. Pharm. Prod.*, vol. 7, no. 2, pp. 80–84, 2012.
- [10] N. Paniel, A. Radoi, and J. L. Marty, "Development of an electrochemical biosensor for the detection of Aflatoxin M1 in milk," *Sensors*, vol. 10, pp. 9439–9448, 2010.
- [11] L. Sibanda, S. De Saeger, and C. Van Peteghem, "Development of a portable field immunoassay for the detection of Aflatoxin M in milk," *Int. J. Food Microbiol.*, vol. 48, pp. 203–209, 1999.
- [12] C. O. Parker, Y. H. Lanyon, M. Manning, D. W. M. Arrigan, and I. E. Tothill, "Electrochemical Immuno-chip sensor for Aflatoxin M1 detection," *Anal. Chem.*, vol. 81, pp. 5291–5298, 2009.
- [13] Y. Wang, J. Dostálek, and W. Knoll, "Long range surface plasmon-enhanced fluorescence spectroscopy for the detection of Aflatoxin M1 in milk," *Biosensors Bioelectron.*, vol. 24, pp. 2264–2267, 2009.
- [14] I. E. Tothill, "Biosensors and nanomaterials and their application for Mycotoxin determination," *World Mycotoxin J.*, vol. 4, no. 4, pp. 361–374, 2011.
- [15] [Online]. Available: <http://www.symphony-project.eu>
- [16] T. Chalyan *et al.*, "Asymmetric Mach-Zehnder interferometer based biosensors for Aflatoxin M1 detection," *Biosensors*, vol. 6, no. 1, p. 1, 2016.
- [17] M. C. Estevez, M. Alvarez, and L. M. Lechuga, "Integrated optical devices for lab-on-a-chip biosensing applications," *Laser Photon. Rev.*, vol. 6, pp. 463–487, 2012.
- [18] C. Ciminelli, C. M. Campanella, F. Dell'Olio, C. E. Campanella, and M. N. Armenise, "Label-free optical resonant sensors for biochemical applications," *Prog. Quantum Electron.*, vol. 37, pp. 51–107, 2013.
- [19] F. Vollmer and L. Yang, "Label-free detection with high-Q microcavities: A review of biosensing mechanisms for integrated devices," *Nanophotonics*, vol. 1, pp. 267–291, 2012.
- [20] M. Ghulinyan, R. Guider, G. Pucker, and L. Pavesi, "Monolithic whispering-gallery mode resonators with vertically coupled integrated bus waveguides," *IEEE Photon. Technol. Lett.*, vol. 23, no. 16, pp. 1166–1168, Aug. 15, 2011.
- [21] R. Guider *et al.*, "Design and optimization of SiON ring resonator-based biosensors for Aflatoxin M1 detection," *Sensors*, vol. 15, no. 7, pp. 17300–17312, 2015.
- [22] A. Samusenko *et al.*, "A SiON microring resonator-based platform for biosensing at 850 nm," *IEEE J. Lightw. Technol.*, vol. 34, no. 3, pp. 969–977, Feb. 1, 2016.
- [23] D. Gandolfi *et al.*, "Role of edge inclination in an optical microdisk resonator for label-free sensing," *Sensors*, vol. 15, pp. 4796–4809, 2015.
- [24] M. Iqbal *et al.*, "Label-free biosensor arrays based on silicon ring resonators and high-speed optical scanning instrumentation," *IEEE J. Sel. Topics Quantum Electron.*, vol. 16, no. 3, pp. 654–661, May/Jun. 2010.
- [25] C. A. J. Damen, R. G. Heideman, G. J. T. Heesink, F. Schreuder, and G. A. J. Besselink, "TriPleX™-based micro ring resonators for food safety applications," in *Proc. Latin Amer. Optics Photon. Conf.*, Cancun, Mexico, 2014, Paper LF2D.1.
- [26] B. Byrne, E. Stack, N. Gilmartin, and R. O'Kennedy, "Antibody-based sensors: Principles, problems and potential for detection of pathogens and associated toxins," *Sensors*, vol. 9, pp. 4407–4445, 2009.
- [27] S. D. Jayasena, "Aptamers: An emerging class of molecules that rival antibodies in diagnostics," *Clin. Chem.*, vol. 45, no. 9, pp. 1628–1650, 1999.
- [28] C. L. A. Hamula, J. W. Guthrie, H. Zhang, X. F. Li, and X. Chris Le, "Selection and analytical applications of aptamers," *TrAC - Trends Anal. Chem.*, vol. 25, pp. 681–691, 2006.
- [29] R. Guider *et al.*, "Sensitivity and limit of detection of biosensors based on ring resonators," *Sensing Bio-Sensing Res.*, vol. 6, pp. 99–102, 2015.
- [30] T. Chalyan *et al.*, "Characterization of SiON microring resonators for biosensing applications," in *Proc. 2015 Int. Conf. Biophoton.*, 2015.
- [31] K. Yoshimoto, M. Nishio, H. Sugasawa, and Y. Nagasaki, "Direct observation of adsorption-induced inactivation of antibody fragments surrounded by mixed-PEG layer on a gold surface," *J. Am. Chem. Soc.*, vol. 132, no. 23, pp. 7982–7989, 2010.
- [32] L. Pasquardini *et al.*, "SPAD aptasensor for the detection of circulating protein biomarkers," *Biosensors Bioelectron.*, vol. 68, pp. 500–507, 2015.
- [33] Comsol. "Wave optics module user's guide," Comsol AB, Stockholm, Sweden. Tech. Rep., 2013.
- [34] M. T. Yaseen, Y. C. Yang, M. H. Shih, and Y. C. Chang, "Optimization of high-Q coupled nanobeam cavity for label-free sensing," *Sensors*, vol. 15, no. 10, pp. 25868–25881, 2015.
- [35] D. C. Stone and J. Ellis, "Stats tutorial - Instrumental analysis and calibration," Dept. of Chem., Univ. of Toronto, Toronto, ON, Canada, pp. 2006–2011.

**Tatevik Chalyan** received the B.S. and M.S. degrees in physics from Yerevan State University, Yerevan, Armenia, in 2010 and 2012, respectively. She is currently working toward the Ph.D. degree in the NanoScience Laboratory, University of Trento, Trento, Italy. In a period of 2011–2014, she worked at LT-PYRKAL CJSC in the Laser Department as a Laser Engineer, where her activities included the assembling and testing solid-state lasers. Her main research interests include laser physics and lab-on-chip biosensors based on asymmetric Mach-Zehnder interferometers and microring resonators with microfluidic devices.

**Laura Pasquardini** received the Graduate degree in physics from the University of Trento, Trento, Italy, in 2000 and the Master's degree in biomaterials from CIRMIB, Trento, Italy, in 2004. She is currently a Researcher at Bruno Kessler Foundation, Trento, where she is involved in the development of micro and nanodevices and biosensors for genomics and proteomics. Her know-how covers different research fields: biointerphases development and characterization, molecular biology, and high resolution imaging.

**Davide Gandolfi** received the M.S. degree from the University of Innsbruck, Innsbruck, Austria. In 2015, he received the Ph.D. degree from the University of Trento, where he was involved in the projects on development and characterization of integrated photonic biochips, for healthcare and food quality control. This includes experimental physics, visible and NIR spectroscopy, microfabrication of silicon photonic chips, microfluidic, FEM simulations of electric fields and liquid flow. Since September 2015, he has been working with BLM Group as a Laser Technology Developer.

**Romain Guider** received the Graduate degree in optoelectronics engineering from the Ecole Nationale Supérieure de Sciences Appliquées et de Technologie, Lannion, France, in 2006, and the Ph.D. degree from the University of Trento, Trento, Italy, in 2009. His doctoral research focused on the study of new nanosilicon waveguides and nanophotonics structures. He was a Postdoctoral Researcher within the Nanoscience Laboratory, University of Trento. His research interests primarily include areas including the design and characterization of new Si-based photonic structures for lab-on-chip applications. He is currently a Project Manager at ALTEN, Paris, France.

**Alina Samusenko** received the Diploma cum Laude degree of an engineer-specialist in telecommunication in Russia, in 2009. In 2010, she moved to Europe, where she completed a two-year Erasmus Mundus Program on Nano and Biophotonics and received the Master's degree in science, technology and health, mention physics and applications. In 2016, she received the Ph.D. degree from the University of Trento, Trento, Italy. She was a Member of the FMPS Unit of the Fondazione Bruno Kessler Institute. Her research activity include the design, fabrication, and characterization of various photonic devices, e.g., optical biosensors, silicon nanocrystal-based LEDs, and integrated photodetectors.

**Manuela Zanetti** received the Ph.D. degree in biochemistry and biophysics from the University of Padua, Padua, Italy. She did a Postdoctoral Research at CNR, Trento, Italy. She won a Marie Curie Fellowship and got an opportunity to do a postdoctoral research at the University of Oxford. Her research interests include defenses and antimicrobial peptides, bacterial proteins.

**Georg Pucker** received the Doctoral degree in technical chemistry in 1996 from the TU-Graz Austria, Graz, Austria. He is a Senior Researcher at the Center for Materials and Microsystems, FBK, Trento, Italy. From 1996 to 2001, he was a Researcher at the Department of Physics, University of Trento, studying optical properties of doped glasses and silicon nanostructures. Since 2001, he is employed at FBK performing research in the fields of nanotechnology, photovoltaics, and integrated photonics.

**Cecilia Pederzoli** received the Graduate degree in biology from the University of Padova, Padova, Italy. She is a Team Leader of The Biofunctional Surfaces and Interfaces Research Group and the Managing Director of the Biomolecular Sequence and Structure Analysis for Health (LaBSSAH), Bruno Kessler Foundation, Povo, Trento, Italy. Since then, she has worked in the field of biochemistry and cell biology, in particular, studying protein interactions to model and natural membranes. She has coordinated 14 scientific projects funded by local and national agencies. She is a Co-organizer of eight congresses and four international schools. Her papers are published in more than 90 papers on international peer reviewed journals. She is a Supervisor of several Master students and Ph.D. students (University of Padova, Torino and Trento).

**Lorenzo Pavesi** is a Professor of experimental physics and the Head of the Department of Physics, University of Trento, Trento, Italy. He leads the Nanoscience Laboratory. He founded the research activity in photonics at the University of Trento. He was the first President and Founder of the IEEE Italian chapter on Nanotechnology. He has directed more than 25 Ph.D. students and more than 30 Master thesis students. During the last years, he concentrated on Silicon photonics. His interests encompass also optical sensors or biosensors and solar cells. Recent development is toward integrated quantum photonics. He is an author or coauthor of more than 300 papers, author of several reviews, editor of more than ten books, author of two books, and holds seven patents. In 2001, the Italian President awarded him the title of Cavaliere for scientific merit. In 2010 and 2011, he was elected as a Distinguished Speaker of the IEEE-Photonics society. He holds an H-number of 52 according to the Web of Science and of 63 according to Google Scholar.